LAWRENCE
LIVERMORE
NATIONAL
LABORATORY

UCRL-PROC-233716

Soft X-ray Mirrors for the Linac Coherent Light Source

M. J. Pivovaroff, R. M. Bionta, T. J. Mccarville, R. Soufli, P. M. Stefan

August 15, 2007

SPIE Optics and Photonics
San Diego, CA, United States
August 26, 2007 through August 30, 2007

Soft X-ray Mirrors for the Linac Coherent Light Source

M. J. Pivovaroff[a], R. M. Bionta[a], T. J. Mccarville[a], R. Soufli[a], and P. M. Stefan[b]

[a]Lawrence Livermore National Laboratory, 7000 East Ave., Livermore, CA 94550, USA;
[b]Linac Coherent Light Source, Stanford Linear Accelerator Center, Menlo Park, CA 94025, USA

ABSTRACT

The Linac Coherent Light Source (LCLS) is a 0.15−1.5 nm wavelength free-electron laser (FEL) being constructed at the Stanford Linear Accelerator Center (SLAC) by a multi-institution consortium, including Lawrence Livermore National Laboratory (LLNL). One of LLNL's responsibilities involves the design and construction of two grazing-incidence mirror systems whose primary intent is to reduce radiation levels in the experimental halls by separating the FEL beam from unwanted high-energy photons.

This paper discusses one of these systems, the Soft X-ray Offset Mirror System (SOMS) that will operate in the wavelength range 0.62−1.5 nm (0.827−2.00 keV). The unusual properties of the FEL beam translate to stringent specifications in terms of stability, material choice and mirror properties. It also precludes using approaches previously developed for synchrotron light sources. This situation has led us to a unique mirror design, consisting of a reflective boron carbide layer deposited on a silicon substrate. In the first part of this paper, we discuss the basic system requirements for the SOMS and motivate the need for these novel reflective elements. In the second part of this paper, we discuss the development work we have performed, including simulation and experimental verification of the boron carbide coating properties, and the expected performance of the final system.

Keywords: free electron lasers, X-ray optics, X-ray mirrors, boron carbide

1. INTRODUCTION

1.1 The Linac Coherent Light Source

To better understand the role and function of the X-ray mirror systems, we begin with a brief description of the Linac Coherent Light Source (LCLS). LCLS is a free-electron laser (FEL) currently under construction at the Stanford Linear Accelerator Center (SLAC). The ∼$400 million (USD) project is funded by the Department of Energy through the Office of Basic Energy Sciences. Institutions that have contributed to the LCLS project include SLAC, Argonne National Laboratory (ANL), Brookhaven National Laboratory, Lawrence Livermore National Laboratory (LLNL), Los Alamos National Laboratory, and the University of California, Los Angeles. Primary roles in the collaboration fall to SLAC, (which is also responsible for leadership of the project), ANL and LLNL.

LCLS utilizes the existing, final 1 km section of the existing linac at SLAC to accelerate an incredibly short and intense electron bunch, produced by a new RF injector. The electrons will be tuned to leave the linac with an energy between 4.6−14 GeV[1] and then traverse ∼130 m through a series of 33 undulators developed by ANL. The process of traveling through these undulators induces self-amplified spontaneous emission (SASE) at a first-harmonic wavelength (energy) of 0.15−1.50 nm (0.827−8.27 keV). After the electrons are removed from the photon path at a beam dump, the FEL and broad-spectrum spontaneous emission continue through the front-end enclosure (FEE) towards a near and far experimental hall (NEH and FEH, respectively),whose centers are located approximately 100 m and 340 m from the exit of the undulator. Figure 1 illustrates the approximate location and dimension of each of these components on top of a topographical map of the existing SLAC site, while Table 1 lists some of the basic properties of the radiation (spontaneous and FEL) produced by the LCLS.

Send correspondence to M.J.P. E-mail: pivovaroff@llnl.gov, Telephone: +1 925 422 7779

Table 1. LCLS properties[†]

Parameter	**0.827 keV (15 Å)**	**8.27 keV (1.5 Å)**
LCLS repetition rate [Hz]	120	120
Peak spontaneous power per pulse [W]	4.1×10^9	73×10^9
Average spontaneous power [W]	0.24	2.2
FEL pulse duration [rms; fs]	137	73
Number of photons in 1st harmonic FEL	12×10^{12}	1.1×10^{12}
FEL width, exiting undulator [FWHM; μm]	81	60
ω, FEL divergence, exiting undulator [FWHM; μrad]	8.1	1.1
Average FEL power [W]	0.23	0.23
Peak FEL power [W]	5×10^9	9×10^9
Peak FEL brightness [photons/s/mm^2/mrad^2/0.1% bw]	0.28×10^{32}	15×10^{32}

[†]FEL parameters are taken from Ref. 2, except for the beam size, which comes Ref. 3, and the divergence, which is computed using the formalism of Ref. 4; spontaneous parameters are taken from Ref. 1.
[*]All FEL quantities are for a saturated SASE beam, per pulse.

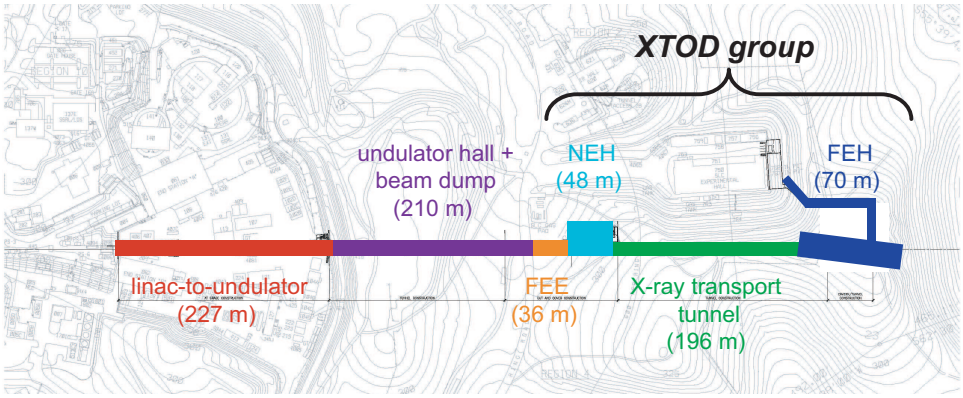

Figure 1. Contour map of the existing SLAC site, with major components of the LCLS indicated by the colored blocks. The XTOD group, led by LLNL, is responsible for infrastructure in the front end enclosure (FEE), the X-ray transport tunnel, the near-experimental hall (NEH) and far-experimental hall (FEH).

1.2 The X-ray Transport Optics and Diagnostics

1.3 Overview

LLNL participates in the construction of the LCLS primarily through the X-ray Optics, Diagnostics and Transport Systems group (XTOD), the organization in charge of design, testing and fabrication of infrastructure and instruments from the far-side of the electron beam dump through the FEH. Figure 2 shows a engineering drawing with the location and size of the various XTOD elements. In broad terms, XTOD is responsible for conditioning the FEL beam, for measuring some of its characteristics as it exits the beam dump and for delivering it to experimental hutches in the NEH and FEH. The diagnostic suite located in the FEE includes attenuators and masks to control the intensity of the FEL, spectrometers and detectors to characterize the shape, amplitude and pulse energy of both the spontaneous and FEL emission and two X-ray mirror systems.

1.4 X-ray mirror systems

The LCLS X-ray mirror systems serve two distinct purposes. The first is to dramatically reduce the amount of high-energy spontaneous radiation, bremsstrahlung γ-rays and their secondary products (*e.g.*, neutrons) within

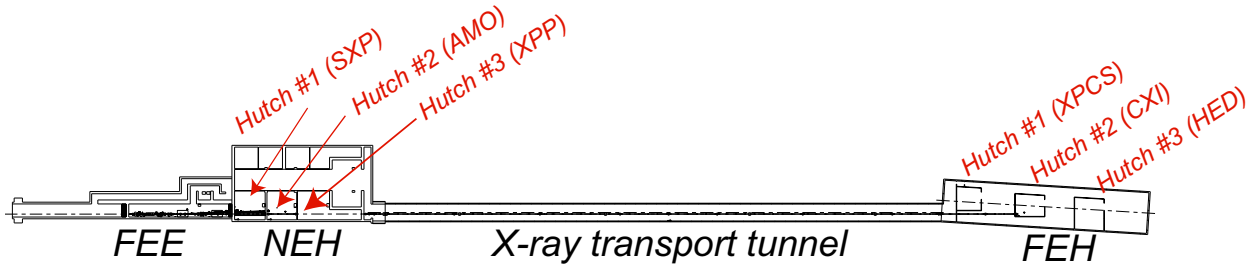

Figure 2. Engineering drawing showing the physical dimensions of the various LCLS sections for which XTOD is building instrumentation.

the experimental hutches located in the NEH and FEH. The second is to physically separate the FEL beam from the spontaneous, broad-band undulator radiation that would contaminate the spectrally-pure SASE radiation (the first-harmonic energies should have a width[1] of $\Delta E/E = [3-7] \times 10^{-4}$). An elegant method for achieving the desired goals relies on grazing-incidence mirrors to act as a low-pass energy filter, efficiently reflecting and deflecting the FEL beam to a trajectory slightly offset from the primary axis of the LCLS facility.

The original 1998 concept study report[5] identified the major research areas that could be advanced by the LCLS FEL, including experiments in basic physics, material science and biology. As both the facility plan and the research goals have matured over the last decade, a design has emerged that provides an experimental end-station (hutch) devoted for each of the following areas: soft X-ray physics (SXP); atomic, molecular and optical (AMO) science; X-ray pump-probe(XPP); X-ray photon correlation spectroscopy (XPCS); coherent X-ray imaging (CXI); high energy density (HED) science. The location of each dedicated hutch depends on the energy range required, coherence properties of the beam and the need for external equipment (*e.g.*, an optical laser for the pump-probe work).

To minimize costs associated with translating experiments out of the FEL path, allowing it to pass to another hutch further down stream, the mirror system is designed to provide several different branch lines. The initial LCLS configuration will contain three unique lines by using a combination of fixed and moveable reflective mirrors and splitting the 0.827−8.27 keV first-harmonic range into two regimes: a 0.827−2.00 keV soft band and a 2.00−8.27 keV hard band. As shown in Figure 3, a total of four mirrors will create two soft branches that will deliver X-rays to the SXP and AMO hutches located in the NEH. Two additional mirrors will create the single hard branch line will initially deliver photons to the XPP hutch in the NEH and the CXI hutch located in the FEH. The remainder of the paper focuses on the Soft X-ray Mirror Offset System (SOMS) that provides two

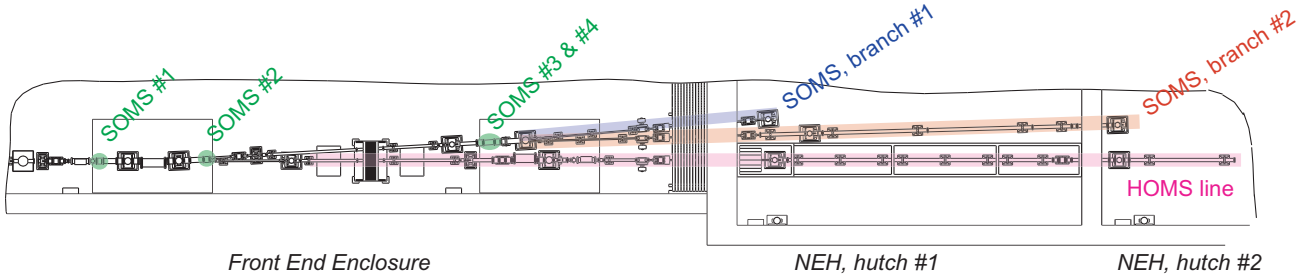

Figure 3. Close-up view of the FEE and first-two hutches of the NEH, indicating the location of the SOMS mirrors and the two soft X-ray branch lines they create.

branch lines in the FEE. In §2, we discuss the basic system requirements for the SOMS, including the desired performance (*e.g.*, the total throughput). Particular attention is given to the requirements that arise due to the unique properties of a 4th generation light source. In §3, we discuss the work undertaken to verify that the system design will meet the specifications, including detailed simulations and calculated properties. In §4, we conclude with the expected performance of the SOMS and summarize the status of the SOMS.

2. SOMS REQUIREMENTS

2.1 Physics requirements

The design of any element instrument or component subsystem for LCLS begins with a physics requirement document (PRD) that describes the goal of the instrument. Engineering specification documents (ESDs) detail how to actually meet the requirements presented in the PRD. Taken together, the SOMS PRD and ESDs cover all aspects of the system including: fundamental requirements (*e.g.*, the operational band-pass), optical requirements (*e.g.*, the finish specification), controls, stability and other opto-mechanical requirements. Below, we present the specific details from these documents relevant for this particular manuscript:

1. **Photon Energy Range**: The SOMS shall operate in the FEL photon energy range from 826.5 eV to 2000 eV
2. **Mirror System Acceptance**: The SOMS shall consist of optical elements sized to accept at least 95% of the FEL radiation cone
3. **Mirror Reflectivity**: The reflectivity of each mirror in the SOMS shall exceed 90% over its required photon energy range
4. **Basic Mirror Geometry**: The SOMS mirrors shall have flat, planar reflecting surfaces
5. **Mirror Surface Specifications**: Mirror surface specifications...shall be designed to limit degradation of FEL divergence and transverse coherence

Error Category	Spatial Frequency	Corresponding Wavelength	Specification
High-spatial roughness	0.5 μm^{-1} to 50 μm^{-1}	20 nm to 2 μm	$\leq$0.4 nm rms
Mid-spatial roughness	10^{-3} μm^{-1} to 0.5 μm^{-1}	2 μm to 1 mm	$\leq$0.25 nm rms
Figure (slope errors)	(mirror size)$^{-1}$ to 10^{-3} μm^{-1}	mirror size to 1 mm	$\leq$0.25 μrad rms
Figure (height errors)	(mirror size)$^{-1}$ to 10^{-3} μm^{-1}	mirror size to 1 mm	$\leq$2.0 nm rms

6. **Overall Materials Specification**: The materials used for the mirrors shall be chosen to withstand long-term incidence of the fully-saturated FEL beam
7. **Reflective Material Specification**: The material which reflects the FEL shall, in addition, have no absorption edges in the photon energy range of operation.
8. **Harmonic Rejection**: The high-photon-energy cut-off is chosen to provide third harmonic rejection...to be effective, the System reflectivity at 2.48 keV must be below 20%.
9. **Beam Degradation**: The SOMS shall not reduce the intensity of the FEL by more than 20% nor broaden its divergence by more than 10%

Although many of these requirements will be discussed at length, here we briefly motivate the underlying purpose of each requirement. Some of the requirements will facilitate experimental fidelity and operation, such as having damage-resistant mirrors that do not require expensive replacement (#6), removing higher-order harmonics that can spectrally contaminate the purity of the FEL radiation (#8) or having smooth, well-behaved reflectivity calibrations that lack the complex structures associated with absorption edges (#7). The criteria on system acceptance, reflectivity and beam degradation (#2,#3 and #9) arise from the desire to provide the science experiments with the highest number of FEL photons as possible. In a similar fashion, the specification on mirror flatness and beam divergence (#4 and #9) aim to provide the highest fluence (photons per unit area). The detailed values for errors in different spatial frequencies (#5), to first order, can influence these other factors. For example, the high-spatial roughness will impact the reflectivity of mirror, while the mid-spatial roughness and slope errors will determine how much the central core of the beam is broadened and how many photons may be scattered in the wings of the PSF. The height errors, on the other hand, will impact the coherence of the reflected FEL beam. Taken together, these specifications drive the SOMS design in three broad areas: the physical length and overall dimensions of the mirrors (§3.2), the quality of the mirror surfaces (§3.3) and the material(s) from which the mirrors are made (§2.2 and §3.4).

2.2 Special consideration for FEL applications

Although the LCLS machine has many similarities to a traditional synchrotron light source, its intense, monochromatic ≤200 fs FEL pulses make it distinctively different from 3rd generation light sources. In fact, the expected brightness (see Table 1) is such that, except for a limited number of low-Z elements, the FEL will instantaneously melt and hence damage most materials. Here, we briefly summarize the results of several authors[4,6,7] who have explored this phenomenon in detail.

Evaluating the potential damage to a LCLS element (*e.g.*, a mirror) requires factoring its composition, location, and the photon density of the FEL beam at that element to compute the absorbed dose, in units of eV/atom, as a function of photon energy. This value must then be compared to several quantities of concern: the dose D_3 that can cause significant material degradation due to a sudden rise in temperature (*i.e.*, thermal fatigue);[6] the dose D_2 required to reach the melting temperature; and the dose D_1 needed to actually melt the material. In general, $D_1 > D_2 > D_3$. Recent experimental work at the FLASH facility[8] (a VUV FEL operating at DESY; Hamburg, Germany), indicates that the instantaneous damage threshold of concern for FEL applications lies somewhere between D_1 and D_2. Figure 4 compares the absorbed dose as a function of position from the end of the undulator for a number of low-Z materials. The vertical band denotes the range of distances where the dose falls between D_1 and D_2. (Although these calculations assume normal-incidence absorption by the FEL, the fact that the SOMS mirrors will be operating at near the critical angle for these materials, means the damage thresholds will be comparable.) This work indicates that even pure Si elements could be damaged by the FEL, limiting candidate mirror materials that can satisfy Specification #6 to Be, B_4C, SiC and Al_2O_3 (not shown to enhance the clarity of Figure 4).

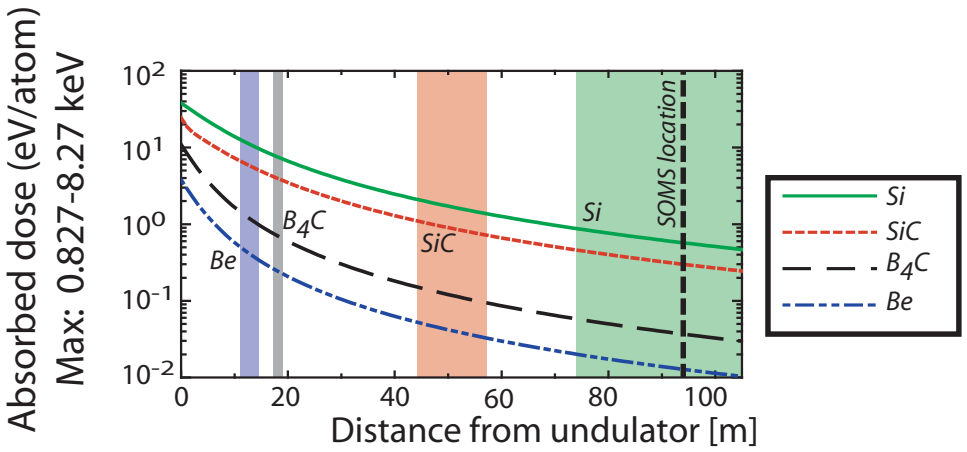

Figure 4. Maximum absorbed dose for Be, B_4C, SiC and Si in the 0.827−8.27 keV energy range, the first harmonic FEL band, versus distance from the end of the undulator. The vertical bands correspond to the distances where the dose falls between D_1 (temperature to melt) and D_2 (temperature to reach melt); that is, the range of distances at which the FEL will damage a material. To guarantee survival, then, an element made from each of these materials must be located at a larger distance (*i.e.*, to the right of the vertical band). For the location of the SOMS, indicated by the heavy dashed line, the only safe material choices are thus Be, B_4C, SiC and Al_2O_3 (not shown, but similar to SiC). Data courtesy of Stefan Hau-Riege; see also Ref. 7.

Safety concerns with the toxicity of beryllium particles eliminate it from further consideration, and Specification #7 precludes SiC and Al_2O_3. This means the only viable candidate for the SOMS mirrors is B_4C. However, while B_4C can be obtained in monolithic pieces, it is impossible to achieve the surface finish required of reflective, grazing incidence optics. As a result, the SOMS X-ray mirrors will consist of a thin, uniform B_4C coating deposited on top of an ultra-smooth, ultra-flat (see Specification #5 for quantitative values) monolithic silicon substrate. This approach heavily leverages surface metrology and thin film deposition facilities and expertise acquired at LLNL during the extreme ultraviolet lithography program (See Ref. 9 and references therein.)

Finally, we note one other extremely important difference between the LCLS and 3rd generation synchrotron light sources. While the peak power is orders of magnitude higher, the average power is orders of magnitude

lower. Consider that the primary optics for the Advanced Photon Source can see upwards of several kW of X-ray power.[10] For the LCLS, the combined FEL and spontaneous radiation deliver, on average, at most a few W. Fortunately, this eliminates the need for incorporating complex cooling mechanisms directly into the mirror substrates (*e.g.*, channels for cooling water machined in the silicon). However, the stringent pointing stability requirements present their own unique challenges that require significant understanding and control of the thermal environment.

3. SOMS SPECIFICATIONS AND PERFORMANCE

Developing a complete design–one that meets the requirements defined in the PRD and ESDs, provides the multiple branch lines that allows efficient use of the FEL in multiple experimental hutches and can survive the extreme conditions of the FEL itself–involved iterating with several groups at SLAC and LLNL and balancing performance goals against state-of-the-art technological capabilities. Below, although we consider various aspects of the SOMS as independent units, this is purely to facilitate presentation of the material. In practice, maximizing performance and utility is only accomplished by simultaneously considering the impacts of all potential design choices.

3.1 Physical layout

As already discussed in §1.4, the SOMS consists of a total of four mirrors. The desired orientation of the two, soft X-ray beam lines requires the FEL beam make a total of three reflections per beam line, all at incident angles of $\theta = 13.9$ mrad. The mirrors are positioned such that the reflective face is parallel to the vertical, an orientation that produces a horizontal deflection of the beam. The first mirror (SOMS1) is set at an angle of θ (and can be translated in the horizontal, to allow the FEL to enter the hard X-ray beam line as needed). The FEL beam reflects at 2θ, intersects the second mirror (SOMS2), which is set at an angle of 3θ. The FEL now approaches the final mirrors (SOMS3, SOMS4) at angle of 4θ. SOMS3 and SOMS4 are positioned on a common translation stage and are set at angles 5θ and 3θ, respectively. This configuration affords a maximum spread between the two branch lines, with one branch line orientated traveling at 6θ, the other at 2θ. Figure 5 show a top-down (plan) view of the SOMS mirrors, using a 10:1 anamorphic scaling.

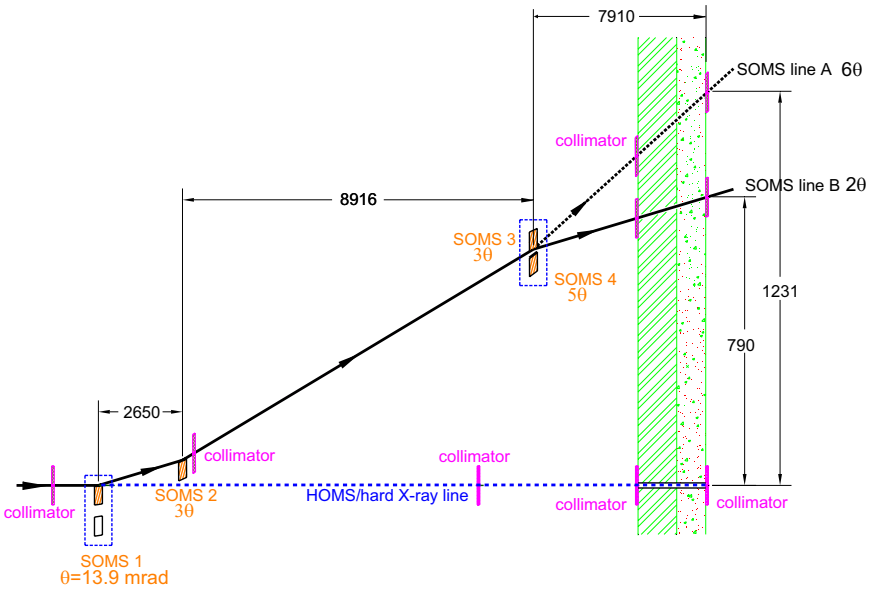

Figure 5. A 10:1 anamorphic plan view of the SOMS configuration, including relative location of the mirrors and the orientation of the two resulting soft X-ray branch lines. Distances are given in mm.

3.2 Length

The clear aperture of the SOMS mirrors is driven by Specifications #2 and #4. Here, we assume the FEL beam is well-described by a 2D gaussian,[4] and we only consider the beam properties at 0.827 keV, since the beam decreases in size and divergence with increasing photon energy. At the location of the SOMS, we calculate that the FEL beam will have a 2D gaussian width $\sigma = 411$ μm, with 95% of the flux contained within the central $4.895\sigma =$ or 2.00 mm of the PSF. When projected at a graze angle of $\theta = 13.9$ mrad, this diameter becomes $4.895\sigma/\theta = 145$ mm. Our calculation must also include for the 0.25 μm shot-to-shot FEL beam jitter of the FEL (*i.e.*, the variation in the pointing of the FEL) and a FEL-proof protective structure attached to the face of the Si substrate. These additional considerations increase the minimum length to 152 mm. We set the final clear aperture length at 175 mm to accommodate potential increases in FEL beam size or divergence during initial LCLS commissioning. The overall dimension of the single-crystal silicon substrate is 250 mm long, 30 mm wide and 50 mm tall, with the clear aperture of 10 mm wide by 175 mm long located in the mirror center. The net surface distortion due to coating, mounting, gravity, and beam heating have been evaluated with finite element calculations, and contribution to figure error is within the scale of initial fabrication errors. The mount is carefully designed to ensure this outcome.

3.3 Figure and finish

By far the most complex aspect of developing the SOMS specification was deriving the limits on roughness, slope and height errors and loss of fluence (Specifications #5 and #9). This requires delicately balancing state-of-the-art manufacturing capabilities against the desire to preserve the coherence, intensity and low-divergence of the FEL beam. The basic steps involved: (1) using recent vendor performance as a starting point for our calculations, (2) predicting the performance of SOMS mirrors of similar quality, (3) having vendors provide coupons manufactured while trying to meet the SOMS specifications and (4) refining the specifications based on the vendor evaluations.

We began by examining metrology data from flat, single crystal silicon mirrors, with clear apertures at least the size of the SOMS mirrors, delivered to SLAC during the last ten years. We computed, $S(f_x)$, the 1D power-spectral density (PSD) derived from interferometric measurements of two mirrors and fit a power-law model of the form:

$$S(f_x) = \frac{K_n}{f_x^n} \tag{1}$$

The data and best-fit model, with ($K_n = 3.81 \times 10^{-9}$ and $n = 1.33$, are shown in the left panel of Figure 6. The good agreement of the data with a power law arises from the well-known fractal behavior of synchrotron mirror PSDs.[11] To be conservative, we increased the multiplicative factor K_n by 3$\times$ to allow for a worst-case scenario that the vendors would deliver mirrors with higher roughness than their most recent products. In calculations presented below, we thus adopt a value for the scale factor of $K_n = 3K_n^{\rm best-fit} = 1.14 \times 10^{-8}$ and power-law index of $n = 1.33$ for our comparator. After discussions with several potential vendors, we also assumed the SOMS mirrors would have a figure error of 0.25 μrad. As we shall see, this assumption is consistent with the PSD used below.

Armed with the PSD, we apply the formalism developed by Church and Tacaks[12–14] to predict how the imperfections will alter the narrow, low-divergence FEL beam. For reference, roughness σ and slope-error μ are computed from these expressions:

$$\sigma^2 = \int_{f_1}^{f_2} S(f_x) df_x \tag{2}$$

and

$$\mu^2 = (2\pi)^2 \int_{f_1}^{f_2} S(f_x) f_x^2 df_x. \tag{3}$$

Another important quantity is the system coherence length,[14] W, a unique spatial wavelength at which imperfections cause scatter into (for lengths longer than W) or out of (for lengths shorter than W)the image core).

$$W = \frac{\sqrt{2}\lambda}{\Theta \cos\theta}, \tag{4}$$

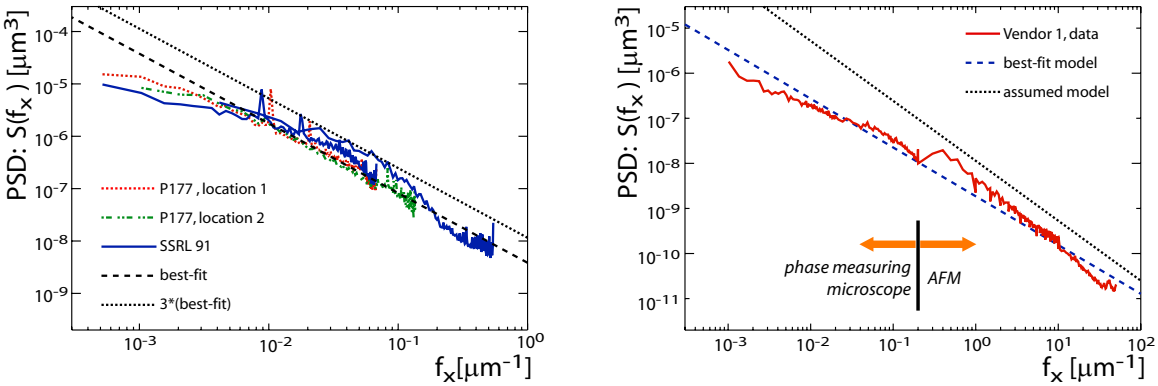

Figure 6. **Left:** PSD of two flat silicon mirrors recently delivered to SLAC. The dashed line is the best-fit model, with scale factor K_n; the dotted line is the comparator model used in the derivation of the specifications, with scale-factor equal to $3K_n$. **Right:** PSD derived from a sample coupon provided by a candidate vendor, attempting to meet the SOMS specifications. The dashed line indicates the best-fit model, while the dotted line shows the power-law model assumed for our calculations. (This is the same dotted lined shown in the right panel.) These data clearly indicate vendors can fabricate mirrors that can meet the SOMS high- and mid-spatial frequency error requirements. Please note the different x- and y-axis ranges between the left and right plots.

where λ is the wavelength of radiation, θ is the graze angle (for the SOMS, $\theta = 13.9$ mrad) and Θ is the angular radius of the incident beam and is related to the FWHM divergence ω reported in Table 1 by $\Theta = 2\omega/2.35$. More informally, W represents the transition from the regime of geometric optics, where figure errors dominate, to that dominated by diffraction induced by higher-spatial frequency roughness.

As shown in Ref. 14, the PSD can be used to calculate the loss of intensity arising from surface imperfections. For radiation reflecting off a single surface with a fractal PSD, it is possible to show that $I_0(0)$,the ratio of on-axis intensity without errors to that with errors, $I(0)$ is given by

$$\frac{I(0)}{I_0(0)} \approx 1 - \left[\frac{8}{\Theta}\mu_1^2\right] - \left[\left(\frac{4\pi}{\lambda}\cos\theta\right)^2 \sigma_1^2\right], \tag{5}$$

where σ_1 is the band-width limited roughness, Equation 2 evaluated at $f_1 = 1/W$ and $f_2 = 1/\lambda$, and μ_1 is the band-width limited slope error, Equation 3 evaluated at $f_1 = 1/(\text{mirror length})^*$and $f_2 = 1/W$. Thus, the first term in the square brackets estimates the losses due to slope errors (*i.e.*, low-spatial frequency errors) and the second term in square brackets represents losses due to surface errors (*i.e.*, mid-to-high-spatial frequency errors). Extending the formalism to multiple reflections, Table 2 reports the approximate percentage loss after each reflection of the SOMS. For a fractal PSD, it is also possible to compute the exact loss in closed form. We also report this value in Table 2. The agreement indicates the assignment of loss due to "finish" (*i.e.*, roughness) or "figure" (*i.e.*, slope) errors is a good assumption.

Table 2. Decrement in FEL beam due to SOMS surface errors[†]

E (keV)	Beam FWHM, ω	One reflection			Two reflections			Three reflections		
		Exact solution	Estimates:		Exact solution	Estimates:		Exact solution	Estimates:	
			Figure	Finish		Figure	Finish		Figure	Finish
0.827	8.1 μrad	8.2%	1.4%	7.3%	16%	2.9%	14%	23%	4.3%	20%
2.00	3.6 μrad	1.4%	0.25%	1.3%	2.9%	0.50%	2.5%	4.2%	0.75%	3.9%

[†]Assuming a fractal PSD with $n = 1.33$ and $K_n = 1.14 \times 10^{-8}$

With specifications described above, the XTOD group approached potential vendors to assess the feasibility of fabricating the silicon substrates. As part of this dialogue, several vendors provided sample coupons to allow

[*]In practice, the actual mirror length has little influence on the calculation of μ_1, since for typical mirrors lengths of $\geq$100 mm, f_1 quickly approaches zero.

us to determine if their manufacturing process would meet the stringent SOMS specifications. Interferometric and atomic force microscopy (AFM) measurements performed at LLNL indicated that a subset of the vendors could in fact deliver the needed quality. The PSD resulting from some of these measurements in shown in the right panel of Figure 6. The mid- and high-spatial frequency roughnesses for this particular coupon had a value $\sigma_{\rm mid} = 0.13$ nm and $\sigma_{\rm high} = 0.11$ nm. The mirror substrates will easily be below the specifications of $\sigma_{\rm mid,spec} \leq 0.25$ nm and $\sigma_{\rm high,spec} \leq 0.40$ nm. However, we must also account for a growth in high-spatial roughness due to the B_4C deposition (see §3.4 for details). The best-fit power-law model, also shown in Figure 6, has parameters of $K_n = 1.86 \times 10^{-9}$ and $n = 1.08$, which is consistent with, but significantly lower than, the comparator fractal model used when deriving the specification. This provides additional confidence that the SOMS mirrors will only minimally degrade the FEL beam (Specification #9), and based on the results in Table 2, the loss of intensity due to the SOMS will be under 20%.

The next task is to calculate how much surface errors will increase the FEL divergence. Again, Church and Takacs[12,14] provide the mathematical framework for describing the changes to an idealized gaussian beam reflecting from a single mirror. Rather than repeat the complex derivation, we briefly summarize the process we have adopted and discuss the *ad hoc* steps used to account for multiple reflections. For a single reflection, the PSD is used to determine the decrement and shape of the scattered wings.[14] This result is then convolved with a gaussian function to account for additional broadening due to slope errors.[11]

For a total of N reflections, we assume the shape of the wings will stay constant, but the amplitude should be multiplied by N. For the core of the point spread function (PSF), we assume that the PSD-derived scattered PSF should be convolved with a composite blur function. This composite function is a gaussian, whose width corresponds to the figure error, convolved with itself N times. This results in two discrete models: one for the central core, another for the broad wings. We then use a spline-fit to combine the two components into a single, comprehensive model of the PSF. Figure 7 compares the PSF at 0.827 and 2.00 keV before encountering the SOMS and after it has been reflected three times. At the lowest energy, the FWHM divergence broadens from 8.1 to 8.2 μrad, an increase of just 1.2%. At the highest energy, the FWHM broadens from 3.7 to 3.9 μrad, an increase of 5.4%. Thus, the SOMS will meet the second part of Specification #9.

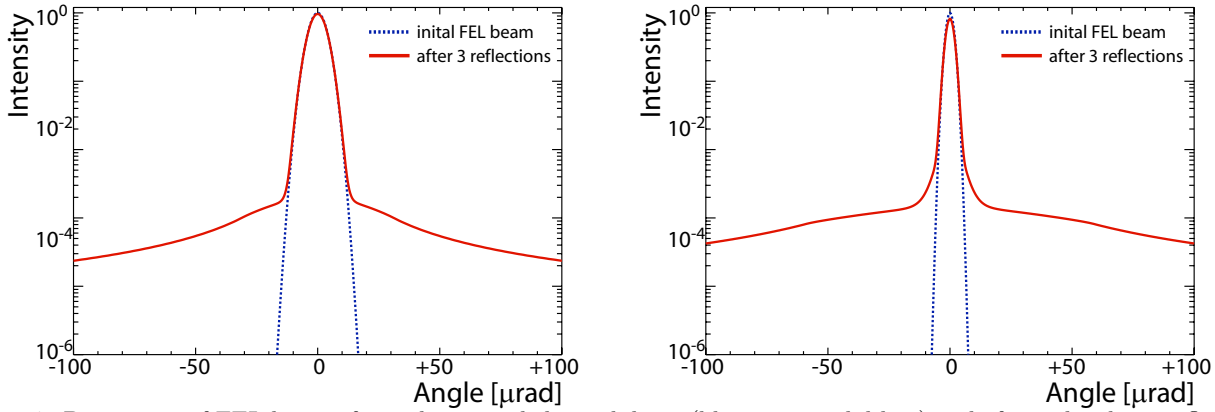

Figure 7. Divergence of FEL beam after it has exited the undulator (blue curve, solid line) and after it has been reflected three times by the SOMS (red curve, dashed line). **Left:** The FEL beam at 0.827 keV. The input PSF core has a FWHM of 8.1 μrad, after exiting the SOMS it has increased to 8.2 μrad. **Right:** The FEL beam at 0.827 keV. The input PSF core has a FWHM of 3.7 μrad, after exiting the SOMS it has increased to 3.9 μrad.

We end our discussion of surface errors with a final consistency check between our assumption of a slope error 0.25 μrad figure and our comparator PSD model. Using the band-width limited definition of rms slope error (Equation 3) and a mirror length of 175 mm (see the discussion in the following section), we compute $\mu_1 = 0.13$ μrad. Because the assumed slope error used in the PSF calculations is larger than that expected from the comparator model, there is an additional margin of safety built into our calculations.

3.4 Coating

As discussed in §2.2, B_4C was chosen as the reflective coating material for the SOMS mirrors due to its damage-resistant nature against the LCLS FEL beam. Boron carbide exhibits exceptionally high hardness (it is the 3rd hardest material after cubic boron nitride and diamond, at room temperature), low specific weight, high impact resistance, and high neutron-absorption cross section. Because of these properties, boron carbide films with varying stoichiometries have found scientific and industrial applications such as armor and wear parts, and neutron absorber elements. Magnetron or ion-beam sputtered B_4C films with thicknesses ranging from a fraction of a nanometer to a few nanometers have been used as barrier or spacer layers in reflective multilayer optics operating in the extreme ultraviolet (EUV)/soft X-ray energy region. For the single-layer, grazing-incidence SOMS mirrors, we have determined through modeling that the optimum thickness of the B_4C coating is 50 nm (see §4 for more details). Although there are many publications on sputtered boron carbide films tailored for the aforementioned applications, there are only a limited number of earlier studies[15–17] on the physical and optical properties of single-layer, sputtered B_4C films deposited as EUV/x-ray reflective coatings. The literature is particularly sparse in the $0.827-2.00$ keV photon energy range of operation, a sign that the experimental performance of grazing-incidence X-ray mirrors with such B_4C coatings has not been investigated previously.

The B_4C reflective coating for the SOMS mirrors must also preserve the figure, mid- and high-spatial frequency properties of the Si substrate specified in the table in Section 2.1. These substrate specifications translate to requirements for low roughness in the mid- and high-spatial frequencies for the B_4C film. Moreover, given that the figure errors of the substrate and subsequent reflective film are uncorrelated and thus add in a quadratic fashion, the thickness uniformity of the B_4C film should be within 1 nm rms (**i.e.,** about half of the substrate figure specification) across the 175 mm mirror clear aperture, in order for the boron carbide film to not contribute to degradation of the mirror figure. The stress of the coating should also be sufficiently low to prevent delamination from the substrate surface and maintain the overall figure deformation of the B_4C-coated mirror within the specification of 2 nm rms. As is the case with all reflective coatings for X-ray optics, the top surface of the boron carbide film should be stable against contamination (oxidation, hydrocarbons), to maintain consistent reflective performance over time.

To investigate the B_4C coating properties for the SOMS mirror application, boron carbide films were deposited at LLNL on clean (100) Si wafer substrates with nearly ideal high-spatial frequency roughness ($\sim$0.05 nm rms). A planar DC-magnetron sputtering system used for large-area, ultra-precise EUV/x-ray coatings[9] was used for these depositions. The same system will ultimately be used for the deposition of the B_4C coatings on the actual SOMS mirror substrates. X-ray Photoelectron Spectroscopy (XPS) on samples aged for about one month indicated that the top 0.9 nm of the films are oxygen- and carbon- rich (atomic percentages: boron = 64%, carbon = 22%, oxygen = 13%) with the oxygen and carbon concentrations rapidly diminishing with increasing depth from the top surface. Rutherford backscattering (RBS) measurements indicated a 3.9:1 boron-to-carbon atomic ratio, with 6% (atomic) oxygen present, averaged across the entire film thickness. Through RBS and EUV reflectance measurements, it was determined that the density of the sputtered films is 2.2 g/cm^3 (88% of the density of the bulk boron carbide crystal). The high-spatial frequency roughness (in the frequency range specified in Table 2) of 50-nm thick B_4C films made using nominal deposition parameters was 0.15 nm rms, measured by AFM. The stress of these films was -2.3 GPa (compressive). Although no delamination was observed on these films, aged for over a year after deposition, this level of stress was predicted to lead to figure deformations exceeding the total error budget of 2 nm rms (SOMS specification), when deposited on the actual SOMS mirror substrates. By modifying the deposition parameters, we produced B_4C films with a factor of 2 lower stress (-1.1 GPa), a level predicted to meet the stringent figure error requirement. The high-spatial frequency roughness of the modified B_4C films was 0.5 nm rms, which marginally meets the SOMS high-spatial frequency roughness requirement. Optimization of the B_4C coating thickness uniformity is currently underway, which will allow us to meet the 1 nm rms height-error specification across the SOMS mirror clear aperture. A detailed description of the B_4C coating development for the SOMS mirrors will be given in a future publication.

4. CONCLUSION

4.1 Predicted performance

We used IMD[18] to optimize the thickness of the boron carbide coating needed to meet Specifications #3 and #8, using the density and stoichiometry we measured (§3.4). Assuming a worst-case film roughness of $\sigma = 0.5$ nm[†], we determined that the minimum film thickness to provide 90% reflectivity across the entire SOMS operating band, while suppressing the 3rd harmonic FEL component, was 50.0 nm. Figure 8 plots reflectivity as a function of photon energy. The final throughput of the FEL beam at the minimum and maximum operating energies of the SOMS is the product of: the cube of the reflectivity, the fraction of the FEL beam captured by the 175 mm clear aperture, and the amount remaining in the central peak. At 0.827 keV, this number is $[(91\%]^3) \times (98\%) \times (77\%) = 57\%$; at 2.00 keV, this number is $[(90\%]^3) \times (100\%) \times (96\%) = 70\%$.

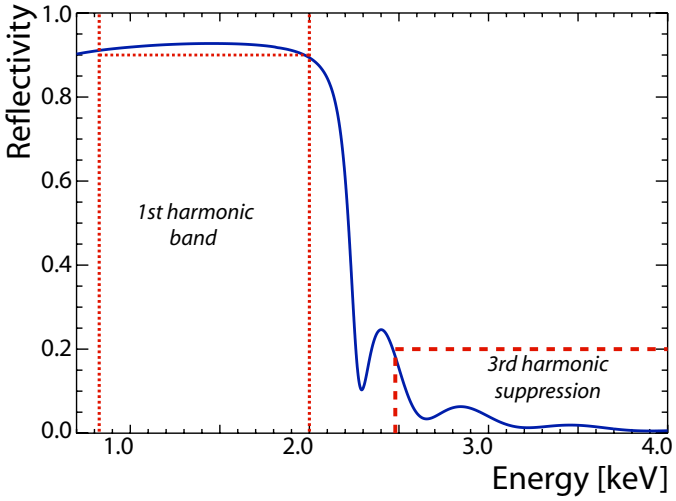

Figure 8. The predicted reflectivity of a 50.0 nm thick boron carbide coating that will be used for the SOMS. The dotted line shows that the reflectivity will be at least 90% in the 0.827−2.00 keV energy band, while the dashed line indicates the reflectivity above 2.48 keV will be below 20% to suppress the 3rd harmonic FEL peak.

4.2 Status

During the summer of 2007, a final vendor was selected to produce the single crystal silicon substrates for the SOMS. Delivery is expected in 2008, at which point the boron carbide deposition will be performed at LLNL. The mirrors will then be integrated into their opto-mechanical assemblies and shipped to SLAC for installation and alignment at the LCLS.

5. ACKNOWLEDGMENTS

This work was performed under the auspices of the U.S. Department of Energy by University of California, Lawrence Livermore National Laboratory under Contract W-7405-Eng-48.

We thank the entire LCLS XTOD group at LLNL for their contributions: Sherry Baker and Michael A. Johnson for precision metrology, Jeff C. Robinson and Mark McKernan for technical and engineering assistance, Pat Duffy for the engineering drawings used in Figure 2 and 3, Stefan Hau-Riege for the melt data used in Figure 4 and Donn McMahon for project management support. We thank Angela Craig, Bruce Rothman and Patrick Schnabel (Evans Analytical Group, Sunnyvale, California) for the XPS and RBS measurements. We also thank Eric Gullikson, Andy Aquila and Franklin Dollar (Lawrence Berkeley National Laboratory) for help with

[†]This IMD variable is comparable to the high-frequency roughness. Although $\sigma_{\text{high}} = 0.5$ nm does not formally satisfy Specification #5, we again adopt a conservative approach, to guarantee the film meet the reflectivity requirement (Specification #3). A lower value of σ_{high} will result in higher reflectivity than we calculate here.

EUV reflectance measurements at beamline 6.3.2. of the Advanced Light Source. Finally, we acknowledge John Arthur (SLAC) for many enlightening discussions.

REFERENCES

1. "LCLS parameter database: FEL PHYSICS / PERFORMANCE." http://www-ssrl.slac.stanford.edu/htbin/rdbweb/LCLS_params_DB_public/.
2. "LCLS parameter database: X-RAY OPTICS / RADIATION SOURCE." http://www-ssrl.slac.stanford.edu/htbin/rdbweb/LCLS_params_DB_public/.
3. H.-D. Nuhn, "private communication." 2007.
4. R. M. Bionta, "Controlling dose to low z solids at LCLS." LLNL report: UCRL-ID-137222; http://www.llnl.gov/tid/lof/documents/pdf/237970.pdf , Jan 2000.
5. The LCLS Design Study Group, "Linac coherent light source (LCLS) design study report." SLAC-R-521; UC-414; http://www-ssrl.slac.stanford.edu/lcls/design_report/e-toc.html, Dec 1998.
6. D. D. Ryutov, "Thermal stresses in the reflective x-ray optics for the linac coherent light source," *Rev Sci Inst* **74**, pp. 3722–3725, 2003.
7. S. Hau-Riege, "Absorbed XFEL dose in the components of the LCLS X-Ray optics." LLNL report: UCRL-TR-215833; http://www.llnl.gov/tid/lof/documents/pdf/325503.pdf, Oct 2005.
8. S. P. Hau-Riege, R. A. London, R. M. Bionta, M. A. McKernan, S. L. Baker, J. Krzywinski, R. Sobierajski, R. Nietubyc, J. B. Pelka, M. Jurek, L. Juha, J. Chalupsky, J. Cihelka, V. Hajkova, A. Velyhan, J. Krasa, J. Kuba, K. Tiedtke, S. Toleikis, T. Tschentscher, H. Wabnitz, M. Bergh, C. Caleman, K. Sokolowski-Tinten, N. Stojanovic, and U. Zastrau, "Damage threshold of inorganic solids under free-electron-laser irradiation at 32.5 nm wavelength," *App Phys Lett* **90**, pp. 173128–1–3, 2007.
9. R. Soufli, R. M. Hudyma, E. Spiller, E. M. Gullikson, M. A. Schmidt, J. C. Robinson, S. L. Baker, C. C. Walton, and J. S. Taylor, "Sub-diffraction-limited multilayer coatings for the 0.3 numerical aperture micro-exposure tool for extreme ultraviolet lithography," *App Opt* **46**, pp. 3736–3746, 2007.
10. W. K. Lee, P. B. Fernandez, A. M. Khounsary, W. Yun, and E. M. Trakhtenberg, "Advanced Photon Source undulator beamline tests of a contact-cooled silicon u-shaped monochromator," *Proc SPIE* **3151**, pp. 208–215, 1997.
11. E. L. Church, "Fractal surface finish," *App Opt* **27**, pp. 1518–1526, 1988.
12. E. L. Church and P. Z. Takacs, "The optimal estimation of finish parameters," *Proc SPIE* **1530**, pp. 71–85, 1991.
13. E. L. Church and P. Z. Takacs, "Specifications of surface figure and finish in terms of performance," *App Opt* **32**, pp. 3344–3353, 1993.
14. E. L. Church and P. Z. Takacs, "Specifications of glancing- and normal-incidence x-ray mirrors," *Opt Eng* **34**, pp. 353–360, 1995.
15. G. M. Blumenstock, R. A. M. Keski-Kuha, and M. L. Ginter, "Extreme ultraviolet optical properties of ion-beam-deposited boron carbide thin films," *Proc SPIE* **2515**, pp. 558–564, 1995.
16. C. Tarrio, R. N. Watts, T. B. Lucatorto, J. M. Slaughter, and C. M. Falco, "Optical constants of in-situ deposited films of important extreme ultraviolet multilayer mirror materials," *App Opt* **37**, pp. 4100–4104, 1998.
17. V. E. Asadchikov, I. N. Bukreeva, A. Duparré, I. V. Kozhevnikov, Y. S. Krivonosova, C. Morawe, M. V. Pyatakhin, J. Steinert, A. V. Vinogradov, and E. Ziegler, "X-ray study of surfaces and interfaces," *Proc SPIE* **449**, pp. 243–264, 2001.
18. D. L. Windt, "IMD: Software for modeling the optical properties of multilayer films," *Computers Phys* **12**, pp. 360–370, 1998.